IEEE Access
Multidisciplinary | Rapid Review | Open Access Journal

Received May 30, 2017, accepted June 19, 2017, date of publication July 14, 2017, date of current version August 8, 2017.

Digital Object Identifier 10.1109/ACCESS.2017.2726997

Lossless Compression in Bayer Color Filter Array for Capsule Endoscopy

SHAHED K. MOHAMMED, (Student Member, IEEE), K. M. MAFIJUR RAHMAN, (Student Member, IEEE), AND KHAN A. WAHID, (Senior Member, IEEE)

Department of Electrical and Computer Engineering, University of Saskatchewan, Saskatoon, SK S7N 5A9, Canada

Corresponding author: Shahed K. Mohammed (shahed.mohammed@usask.ca)

This work was supported in part by the Natural Science and Engineering Research Council, Canada, in part by the Canada Foundation for Innovation, and in part by the Western Economic Diversification Canada.

ABSTRACT This paper presents a compression algorithm for color filter array (CFA) images in a wireless capsule endoscopy system. The proposed algorithm consists of a new color space transformation (known as YLMN), a raster-order prediction model, and a single context adaptive Golomb–Rice encoder to encode the residual signal with variable length coding. An optimum reversible color transformation derivation model is presented first, which incorporates a prediction model to find the optimum color transformation. After the color transformation, each color component has been independently encoded with a low complexity raster-order prediction model and Golomb–Rice encoder. The algorithm is implemented using a TSMC 65-nm CMOS process, which shows a reduction in gate count by 38.9% and memory requirement by 71.2% compared with existing methods. Performance assessment using CFA database shows the proposed design can outperform existing lossless and near-lossless compression algorithms by a large margin, which makes it suitable for capsule endoscopy application.

INDEX TERMS Wireless capsule endoscopy, color filter array, lossless image compression, reversible color transformation.

I. INTRODUCTION

Wireless capsule endoscopy (WCE) is a pill-size camera swallowed by the patient for gastrointestinal diagnosis. The camera travels the gastrointestinal tract in a similar fashion to ingested food, captures images along the entire journey and sends these images wirelessly to the recorder outside [1]. WCE has been playing an important role in gastrointestinal disease management by allowing non-invasive and patient-friendly monitoring of digestive tract. Particularly, WCE serves as the first line modality in the diagnosis of obscure gastrointestinal bleeding (OGIB), unexplained iron deficiency anemia (IDA), small bowel mucosal lesions, Chron's disease and Celiac disease [2]. Current researches are going on the development of next-generation wireless capsule with tools to perform biopsies, drug-delivery, and active locomotion. With these tools, WCE has the potential to replace standard diagnostic endoscopy within the next 15 years [3]. However, the bottleneck of WCE is the image quality, image transmission power and battery life [4]. Preserving the image quality by the use of lossless image compression could yield better performance from both manual and computer assisted reviewing process [5]. However, self-powered battery and long transit time limit the image resolution and the frame rate of WCE. Therefore, keeping the image quality high while reducing the transmission power and bandwidth is a challenge.

The image sensors in WCE mostly utilize Bayer color filter array (CFA) to capture the color information with only single sensor plane [6]. Later, a full-color image is produced by a pre-processing method called demosaicing stage, which interpolates the missing colors. However, demosaicing stage increases the redundancy in the image without adding any information. Furthermore, application of a suboptimal low complexity demosaicing stage severely degrades the image quality by introducing artificial color artifacts [7]. In WCE, this leads to degradation of critical findings in the mucosa layer, villous pattern, and underlying blood veins [8], [9]. A lossless transmission of the raw CFA data allows the use of a high complexity edge preserving demosaicing algorithm in the workstation. Additionally, as these images contain

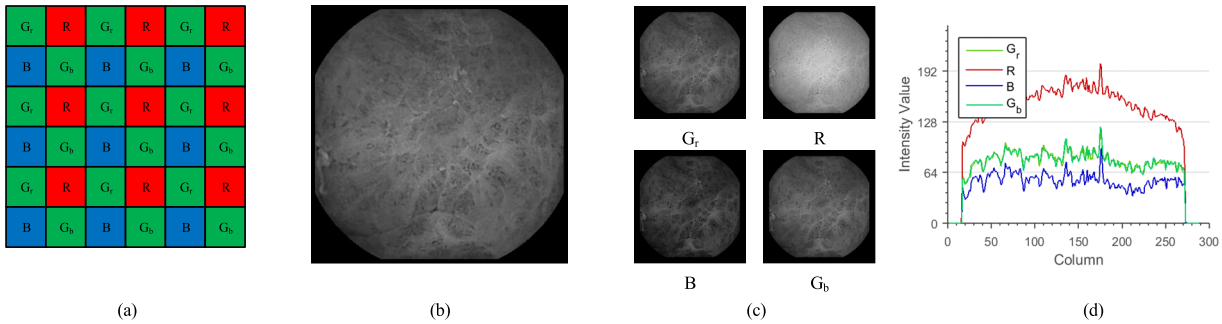

FIGURE 1. A typical CFA image in capsule endoscopy, (a) Bayer Pattern, (b) Mosaic Image, (c) Sub-images generated by separating the color components, (d) Line plot showing the color channel along row 100 in each sub-image to show the redundancy between the color components.

medical diagnostics, archiving them according to Picture Archiving and Communication system requires the lossless distortion [10]. Standard lossless compression engine such as JPEG-LS, JPEG-2000, JPEG-XR or HEVC Intra coding are not feasible for this task due to their computationally expensive design and inferior performance in coding CFA image. Therefore, a dedicated lossless compression scheme for capsule endoscopic image is sought in many of the works.

Several lossless compression methods for wireless capsule endoscopy are proposed in the recent years [10], [11]. However, these methods operate on the full-color image and ignore the error generated and complexity added in the demosaicing stage. There are few near-lossless compression methods proposed for CFA endoscopic images that utilize JPEG-LS lossless algorithm along with a deinterlacing filter to independently code the different color components in CFA image [12]–[14]. However, these algorithms require a buffer memory for storing the context model. As well as the correlation between color components is not sufficiently exploited in these algorithms.

Recently, Malvar et. al. has proposed an optimum color transformation termed as YDgCoCg [15]. By exploiting the inter-color correlation in the CFA image through color transformation, they have demonstrated an improved lossless compression rate for transform based code such JPEG-2000 and JPEG-XR. Similarly, an optimum color transformation that can capture the unique characteristics in endoscopic CFA image can lead to a better image compression with a simple coder.

In this paper, we have proposed a low complexity image compression system for CFA endoscopic image. Our main contribution is the color space derivation model based on the prediction model and entropy coder. This derivation model gives a separable color space transformation termed as YLMN, which can completely exploit the inter-color correlation in CFA image. Furthermore, as YLMN is separable, it can work directly on the raster order data, leading to very efficient implementation. Based on YLMN, we have proposed a low complexity lossless image compression system for wireless capsule endoscopy system. The proposed encoder uses a simple delta pulse coded modulation (DPCM) based prediction model with a low complexity adaptive Golomb-Rice encoder to entropy code the residual signal. The exclusion of high complexity prediction models such as median edge prediction, context modeling, and Huffman encoder lowers the hardware implementation cost in terms of computational resource and memory.

In the experiments, the proposed method is compared with different lossless compression algorithms for both RGB and CFA endoscopic image. The results show that our proposed method yields the best performance among the existing method and standard lossless engine for the endoscopic image. We have compared the results for some simulated CFA image of a high-quality endoscopic image with various conditions such as ulcer, celiac disease. These comparisons show that the proposed method outputs the lowest lossless bit rate on all the images.

II. MATHEMATICAL DERIVATION OF ORCT DERIVATION

A typical CFA image generated by Bayer pattern (Fig. 1(a)) is presented in Fig. 1(b). The Bayer pattern consists of repeating 2×2 macroblock with two green components, one red component, and one blue component. Therefore, a natural way to compress the CFA image is to separate the image into several sub-images consisting of the different color components. For example, by taking a pixel from each 2×2 macroblock, we can get four sub-images comprising two green images, one red image, and one blue image. These sub-images exhibit a high degree of correlation between them similar to the correlation between color channels in RGB image. For example, row 100 for each sub-image has been plotted in Fig. 1(d), showing that the similarity in the color components. Our goal is to design a color space transformation that can reduce the redundancy between these sub-images and improve the coding performance.

There are two ways we can transform the components in 2×2 macroblock in CFA image as illustrated in Fig. 2. We can use a non-separable filter by ordering the components in the 2×2 macroblock lexicographically and apply a 4×4 transform matrix (Fig-2(a)). In the second method shown in Fig. 2(b), we can apply a separable filter, where each column and each row is considered as a 1-D signal and

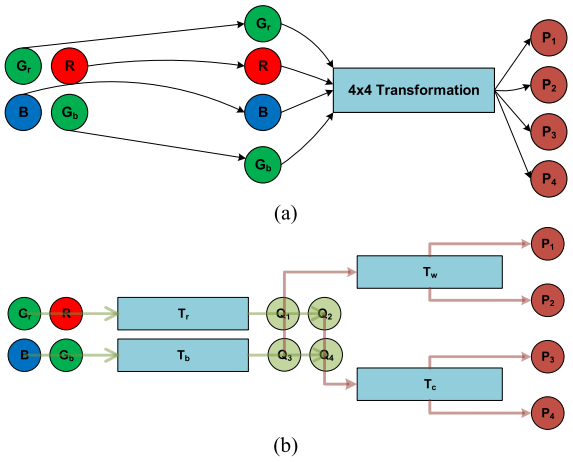

FIGURE 2. Workflow of (a) Non-separable color transformation and (b) Separable color transformation.

1-D transformation are used to map the components into a new color space as shown in eqn(1):-

$$\begin{bmatrix} P_1 & P_2 \\ P_3 & P_4 \end{bmatrix} = T_C \begin{bmatrix} G_r & R \\ B & G_b \end{bmatrix} T_R \tag{1}$$

where T_c and T_R are the column and row transformation matrix respectively. The advantage of the latter approach is lower implementation cost. It also allows subdividing the color derivation by deriving 2×2 row transformation matrix and 2×2 column transformation matrix. We can formally define the color space derivation as determining a matrix A of dimension 2×2 with four coefficients.

$$A = \begin{bmatrix} a_{11} & a_{12} \\ a_{21} & a_{22} \end{bmatrix} \tag{2}$$

To ensure integer-reversible color transformation matrix, we employ the Generalized S-transform framework [38]. According to this framework, A must be unimodular and one row of A should contains only integer coefficients [38]. If the determinant of A is lower than one, there is an essential reduction of data, which leads to distortion in the reconstruction. One of the transformation will be the luminance signal or the approximate signal that contain the major portion of the signal variance. The second output signal will be a chrominance signal, where the coefficients will have equal but opposite magnitude [16]. Combining these conditions leads to the derivation of the following matrix for each 2×2 matrix that has only one unknown parameter α :-

$$A = \begin{bmatrix} \alpha & 1-\alpha \\ 1 & -1 \end{bmatrix} \tag{3}$$

For example, say the two components that need to be transformed are X and Y. The outputs of the transform are W and D. If now the residual signal of these components are respectively dX, dY, dW, dD, then we can express dW and dQ in terms of α :-

$$dW = \alpha dX + (1-\alpha)\, dY \text{ and } dD = dX - dY \tag{4}$$

The goal of the color transformation is to reduce the intra-spectral redundancy between the residual signal dW and dD. We have represented the intra-spectral redundancy with the correlation value expressed as:-

$$J_{corr} = \frac{\text{cov}(dW, dD)}{\sqrt{\text{var}(dW)\text{var}(dD)}} \tag{5}$$

On the other hand, the coding performance of a prediction-based system depends on the accuracy of the prediction model, which can be represented by the variance of the residual signals. For example, the rate-distortion performance of a scalar quantizer based coder for a stochastic signal X can be written as [17]:-

$$D(R) = \xi^2 \sigma_x^2 2^{-2R} \tag{6}$$

where D is the distortion, R is the rate, ξ is a distribution dependent constant and σ_x^2 is the variance of the signal X. Therefore, to represent the cost of prediction error, we have used the variance of the residual signal, which can be expressed as:-

$$J_{pred} = \left((\alpha^2+1)S_x + 2(\alpha(1-\alpha)-1)S_{xy} + \left(1+(1-\alpha)^2\right)S_y\right) \tag{7}$$

where $S_x = \frac{1}{N}\sum_{i=1}^{N} dX_i^2$, $S_y = \frac{1}{N}\sum_{i=1}^{N} dY_i^2$ and $S_{xy} = \frac{1}{N}\sum_{i=1}^{N} dX_i dY_i$

To combine these two cost functions, we have used the Lagrange multiplier as shown in eqn (8):-

$$J = J_{corr} + \lambda \times J_{pred} \tag{8}$$

The model in (8) is qualitatively supported by the experimental results as shown in Fig. 3. We plot the cost functions as a function of the parameter α for the Lena image. All the residual signals are estimated using the DPCM prediction model. If we denote the sub-image as X, then DPCM residual signal is defined by eqn (9):-

$$dX(i,j) = X(i,j) - X(i,j-2) \tag{9}$$

We apply this prediction model for the R-line in CFA image which contains R components and G_r components. We also plot the entropy of the residual signal using a color transformation defined with the parameter α. The observed curves all has a minima close to 0.5, which indicates the minima of the model (8) corresponds to the minima of lossless compression rate represented by the entropy.

A. ORCT FOR WCE

Deriving image-wise ORCT will introduce a substantial increase in computational overhead in the capsule compression system. Instead, we derive the optimum color transformation in offline, by using an extensive endoscopic image dataset. The dataset contains 200 images taken for different

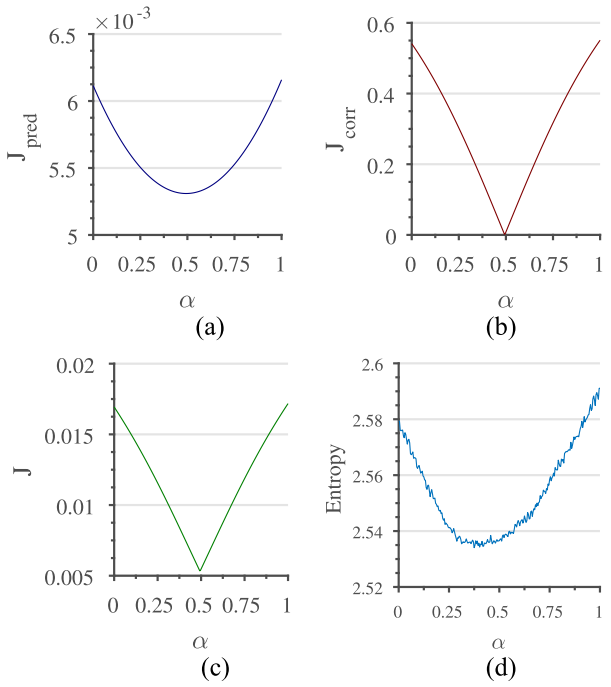

FIGURE 3. Variation of cost functions and entropy with respect to α for Lena image (a) Normalized error variance; (b) Cross-correlation; (c) Total cost (d) Entropy of error signal in all cases minima occurs at 0.5.

condition and location in capsule endoscopy. To derive the color transformation, we apply exhaustive search method to minimize the cost function defined by eqn. (8). First, we derive the row transformation matrix for R-line and B-line in the CFA image. The residual error signal was determined using the DPCM predictor as defined in eqn (9). The resultant transformation matrices are shown in eqn (10) and (11):-

$$\begin{bmatrix} W_r \\ D_r \end{bmatrix} = \begin{bmatrix} \frac{1}{2} & \frac{1}{2} \\ -1 & 1 \end{bmatrix} \begin{bmatrix} G_r \\ R \end{bmatrix} \tag{10}$$

$$\begin{bmatrix} W_b \\ D_b \end{bmatrix} = \begin{bmatrix} \frac{1}{2} & \frac{1}{2} \\ 1 & -1 \end{bmatrix} \begin{bmatrix} G_b \\ B \end{bmatrix} \tag{11}$$

To calculate the column transformation matrix, the outputs of the row transformation matrix are fed again to the derivation model as inputs. The results showed that for difference signal, the original signal contains the lowest entropy. This indicates that R-G and G-B have a lower correlation. However, the weighted signal contains a high amount of correlation, which can be reduced by using the column transformation matrix. The resultant column transformation matrices are shown in eqn (12) and (13).

$$\begin{bmatrix} Y \\ L \end{bmatrix} = \begin{bmatrix} \frac{1}{2} & \frac{1}{2} \\ 1 & -1 \end{bmatrix} \begin{bmatrix} W_r \\ W_b \end{bmatrix} \tag{12}$$

$$\begin{bmatrix} M \\ N \end{bmatrix} = \begin{bmatrix} 1 & 0 \\ 0 & 1 \end{bmatrix} \begin{bmatrix} D_r \\ D_b \end{bmatrix} \tag{13}$$

We denote the color transformation as YLMN. Fig. 4 shows the signal flow graph of YLMN color transformation, while Fig. 5 shows the four resultant sub-images. We also plot the line 100 for each sub-image to demonstrate the reduction in correlation between the signals. Observed plots indicate that the YLMN color transformation has condensed a major portion of the variance into the Y channel. We plot the surface of each sub-image in Fig. 6. It shows that three channels L, M, and N are very smooth and contain mostly low variance chrominance information. Since intra-spectral redundancy is reduced, lower lossless bit rate is expected.

III. YLMN BASED LOSSLESS IMAGE COMPRESSION FOR WCE

Fig. 7 illustrates the block diagram of the proposed lossless encoder based on the proposed YLMN color transformation. The encoder consists of YLMN color transformation, structure separation, a simple delta pulse coded modulation prediction model and a single context adaptive Golomb-Rice encoder. For the input Bayer CFA image shown in Fig. 1(b), first each R-line and B-line is transformed using the row transformation matrices defined in eqn (10) and (11) respectively. The difference signal generated in this step are sent directly to the prediction model. On the other hand, the weighted average signals are stored in buffer memory for further processing using the column transformation matrix defined in eqn (12). This transformation reduces the inter-color redundancy between the color components. After the color transformation, a structure separation stage divides the images into four sub-images, where each sub-image contains pixels from one color plane. This step removes the artificial discontinuities between the pixels. Then each sub-images pass through a DPCM prediction model, which produces the prediction error signal dY, dL, dM and dN. Note that, the prediction model works in raster order fashion and does not require any line buffer. Therefore dM and dN, which are generated in raster order fashion, can be processed in raster order fashion. The details of the color transformation, structure separation, and prediction model will be discussed in this section. Finally, a low complexity but efficient Golomb-Rice Encoder code the error signal generated by the prediction model to produce the bit stream. The bit stream is then sent wirelessly using the RF transmitter to the data recorder located outside of the body.

A. STRUCTURE SEPARATION

After the YLMN color transformation, the proposed scheme deinterleaves the color components into four sub-images. As previously mentioned in Section-II, direct compression of CFA image is not efficient as the mosaic arrangement of the color pixel produces artificial high frequencies. By deinterleaving the CFA image, four downsampled sub-images can be extracted. This deinterleaved procedure removes the artificial high frequencies and therefore improves the compression performance. In previous CE image compression systems [12], structure separation was achieved by shifting the G components to the left of the frame and shifting the R and B components to the right of the frame as shown in

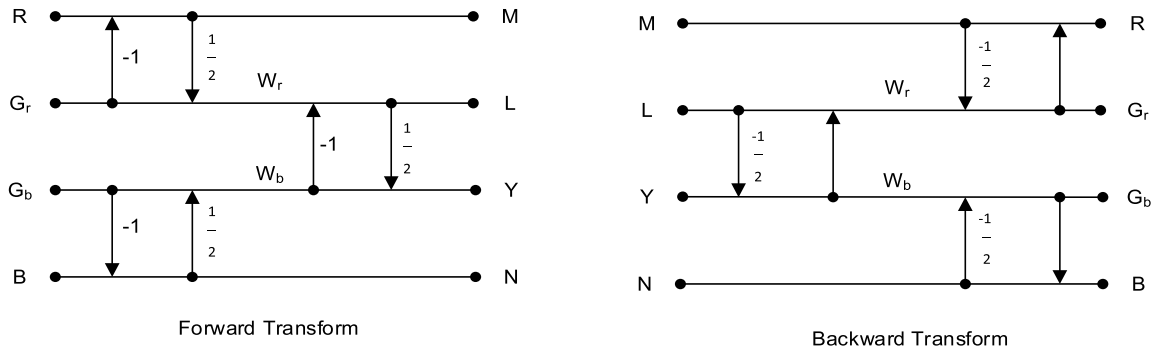

FIGURE 4. Flowgraph of the proposed reversible color transformation ORCT-1 and ORCT-2.

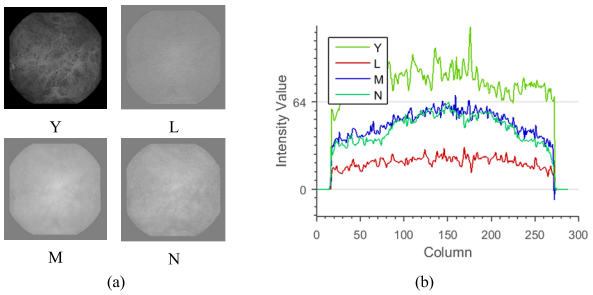

FIGURE 5. Color decomposition in the proposed YLMN colorspace. (a) The color components, (b) The line plots showing the row 100 in each sub-images to demonstrate the reduction in correlation between the transformed color space.

Fig. 8(a). However, due to the high buffer memory requirement, this arrangement is not suitable for hardware implementation. Therefore, instead of rearranging the components in original CFA image, we have changed the prediction model to generate prediction from same color components as shown in Fig 8(b). This reduces the frame memory requirement and leads to a low-memory implementation in VLSI.

B. DPCM

The compression efficiency of predictive coding depends on how accurate the prediction model can predict. Simple linear predictor often generates significant error around the edge areas. To achieve high prediction performance in the edge area, high complexity techniques such as template matching [18], hierarchical prediction [19] and context matching [20] have been employed in lossless CFA compression. However, these techniques require a high amount of frame memory and computational complexity. On the other hand, CE images have a larger smooth area than natural images [21]. Therefore, in comparison to simple prediction model, the improvement of coding performance by high-complexity prediction technique is not significant enough to justify the increase in compression overhead. Simple prediction models such as delta pulse coded modulation (DPCM) prediction model have shown impressive performance in terms of computational complexity and lossless compression ratio in capsule endoscopic image [10], [11]. The proposed prediction model achieves a high prediction performance by exploiting the smoothness of the endoscopic CFA image after the YLMN color transformation. It utilizes the horizontal prediction to handle the pixel in a conventional raster scan order without any buffer memory. To address the discontinuity between the neighboring pixels in CFA images, the prediction template is changed as shown in Fig 8(b). In our model, prediction value is generated from nearest pixel from the same color plane in the horizontal direction using eqn. (9). As the application of YLMN transformation takes into account the inter-color correlation, independent encoding of the deinterleaved sub-images using eqn. (13) yields near optimal compression performance for CE images.

C. GOLOMB-RICE ENCODER

This section presents the single context Golomb-Rice encoder for our compression system. In designing a prediction encoder, it is important to reduce the energy of the residual signal as much as possible. The YLMN transformation and the DPCM prediction model accomplish this goal by reducing the intra-spectral and inter-spectral redundancy. In addition, if the probability distribution function (pdf) of the residual signal can be correctly estimated, we can further reduce the entropy and thus enhance the compression performance. Therefore, we have used a single context for each sub-images, to estimate the pdf of a residual signal continuously while coding the residual signal. The principal of the Adaptive Golomb-Rice coder used here is similar to JPEG-LS encoding [22]. However, instead of using 365 contexts for each color plane, our encoder only utilizes one context for each color plane. This modification results in a drastic reduction of computational complexity and memory. The algorithmic description is given in Fig 9.

As the different color components in the YLMN color space have different characteristics and statistical properties, they are encoded separately with separate context. First, the residual signal is converted to a non-negative number using a mapping function. Then the Golomb-Rice coding [23] transforms the number into two strings. The first strings is an unary

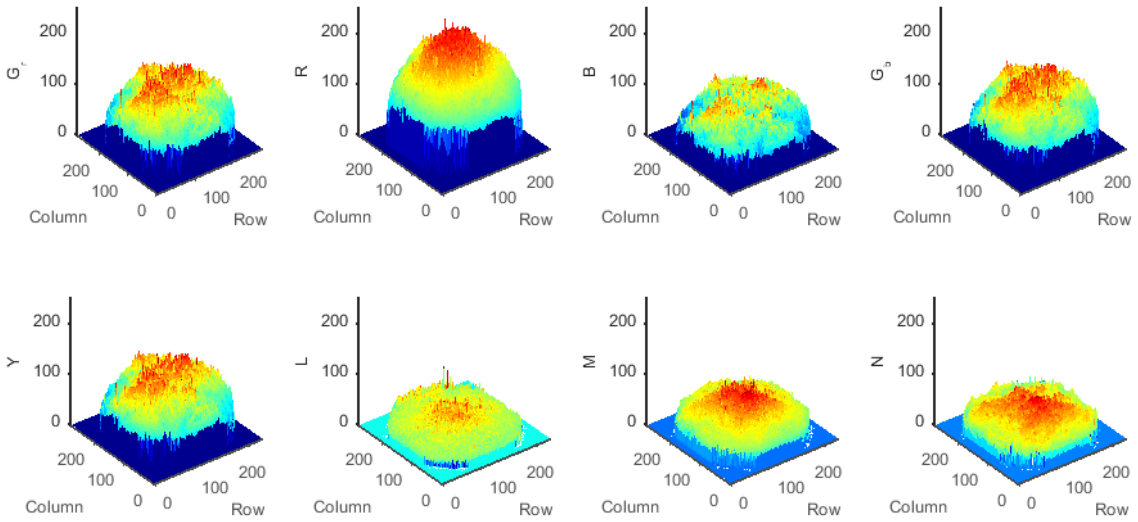

FIGURE 6. Surface plot of the original color components and transformed color components, showing the smoothness in the transformed chrominance components.

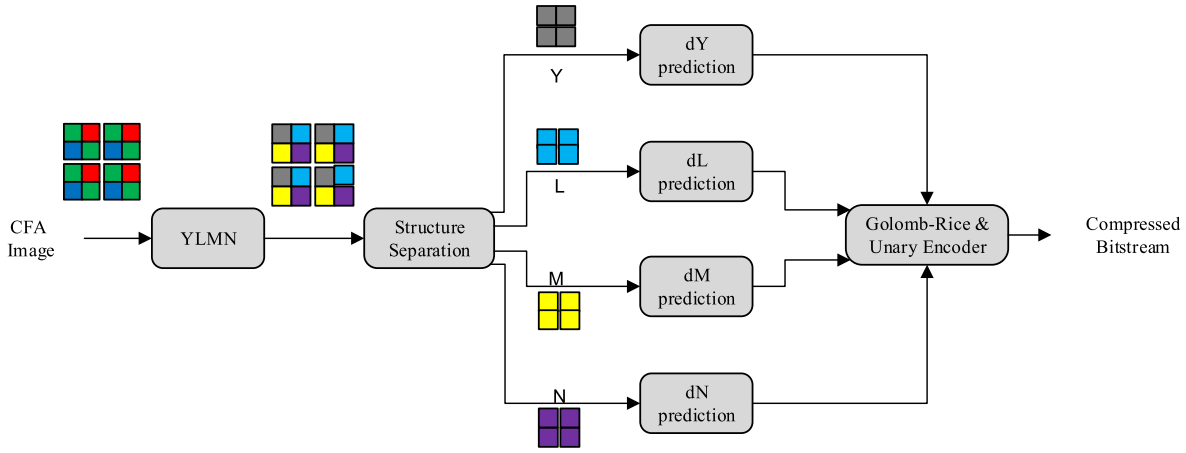

FIGURE 7. Block diagram of the proposed lossless compression algorithm.

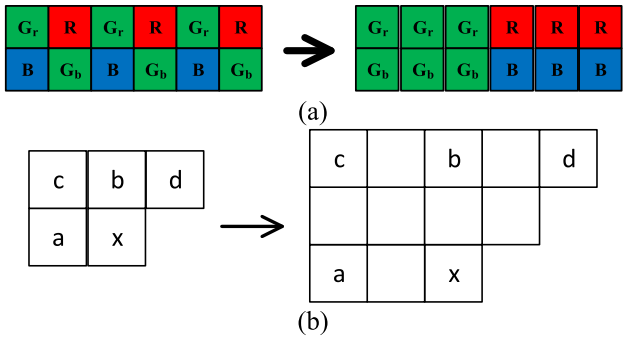

FIGURE 8. (a) Structure separation using rearrangement of the pixels, (b) Structure separation achieved by modifying the prediction template.

representation of the quotient $\left\lfloor \frac{M}{2^k} \right\rfloor$ as the prefix, while the second string is the fixed length code of the remainder. The codelength for residual error dX is $\left\lfloor \frac{2|dX|}{2^k} \right\rfloor + k + 1$.

The parameter k is continuously updated based on the statistics of the signal using two registers to count the number of occurrences (N_c) and accumulate the error (A_c). To reduce the implementation cost, a threshold value $N_{Threshold} = 8$ was used. If N_c becomes greater than this threshold value, both N_c and A_c were halved.

D. CORNER CLIPPING

We have utilized the corner clipping mechanism presented in [24] to discard the dark corner regions in the CE images. This allows us to code the corner regions without any bits. As the size of the image and the shape of the corner region is known, the decoder can reconstruct the image using the bit-stream. Therefore, this is an essentially a lossless mechanism.

IV. PERFORMANCE ANALYSIS

In this section, the performance of the proposed image compression algorithm is assessed and compared with

Algorithm:- Encoding of Residual Error

Inputs: dY_{ij} : Prediction Error

Outputs: S_Y : Bitstream for Y

%% Mapping to Non-Negative Integers

if $dY_{ij} \geq 0$ **Then**

$M \leftarrow 2 \times dY_{ij}$

else

$M \leftarrow 2 \times abs(dY_{ij}) - 1$

end

%% Parameter k Estimation for Golomb-Rice

$k \leftarrow 0$

while $N_c \times 2^k \geq A_c$ **do**

$k \leftarrow k + 1$

end

%% Golomb Rice Coding to convert into variable length bitstream

$S_Y \leftarrow Golomb\_Rice(M, k)$

%%Update Context Parameter N_c and A_c

$N_c \leftarrow N_c + 1$

$A_c \leftarrow A_c + abs(dY_{ij})$

if ($N_c > N_{Threshold}$) **Then**

$$N_c \leftarrow \frac{N_c}{2}$$

$$A_c \leftarrow \frac{A_c}{2}$$

end

FIGURE 9. Pseudo-code for the proposed algorithm for residual signal encoding. It shows the encoding of the Y components. The encoding of L, M, and N also follows a similar procedure with different N_c and A_c values to store their context. Here, Golomb_Rice function returns the bitstream to code the value M with parameter k using a Golomb-Rice, entropy coder.

other lossless compression method developed for capsule endoscopy compression as well as lossless compression method such as JPEG-LS and JPEG-2000. Experiments are carried out using 100 images taken from KID Database [25]. 20 example images are shown in Fig. 10. This database is chosen because it is a publicly available database that contains capsule endoscopic images taken from a wide variety of location from gastrointestinal tract. All the images in the database are captured by Mirocam and stored in full resolution of 360 × 360 [5]. The full-color RGB images in the database are sampled by the Bayer CFA pattern to produce the simulated CFA grayscale image. Performances of different lossless methods are evaluated by comparing compression rate (CR). The CR is reported in bits per pixel (bpp), which is defined as the ratio of the output bitstream in bits and the total number of pixels in the image.

A. COMPARISON OF THE GRBG AND YLMN COLOR SPACE

This section compares the compression performance of the original GRBG channels and the proposed YLMN color space. For the first 5 test images in our database, Fig. 11 shows bar chart of the standard deviation of each sub-images in GRBG color space and the YLMN color space. The height of each bar represents the standard deviation of the corresponding sub-image. Fig. 11 shows that YLMN color transformation significantly reduces the standard deviation of the sub-images, particularly for L, M, and N channels. As lower standard deviation indicates smooth image, it is expected that L, M, and N-channel will result in a lower compression bitrate. As shown in Table 1, the lossless compression rate is reduced particularly for L and N channels.

TABLE 1. Lossless bitrate of the proposed compression scheme with original GRBG color space and YLMN color space.

Image	Gr	R	B	Gb	Y	L	M	N
1	4.33	4.34	4.26	4.32	4.21	3.84	4.31	4.15
2	4.08	4.21	3.98	4.05	3.95	3.70	4.16	3.97
3	4.00	4.04	3.88	3.99	3.87	3.57	3.98	3.91
4	4.31	4.38	4.12	4.25	4.14	3.80	4.23	4.21
5	3.75	3.96	3.83	3.72	3.66	3.44	3.89	3.74

B. COMPARISON OF VARIOUS PREDICTION MODEL

In our model, we have chosen the prediction model based on the trade-off between computational complexity and prediction accuracy. In order to investigate the influence of the prediction model on coding performance, we examine two median edge prediction (MEP) model. First median edge predictor, which we denote MEP1, is widely used as a part of the JPEG-LS compression engine [22]. MEP1 consists of a flat region detector along with a causal template based median edge detection circuit to predict the current pixel from the neighboring pixels. In addition, we also assess the median edge prediction model presented in [26], which we denote as MEP2. MEP2 discards the flat region detection to reduce the computational complexity. Both these two model is applied on the original CFA image where the context model is modified according to Fig. 8. We have applied our prediction model on the original CFA image and the YLMN image. Fig. 12 shows the performance in terms of prediction gain and entropy of the residual signal.

The prediction gain is defined as the ratio between the variance of the original signal to the residual signal measured as shown in eqn 14:-

$$G_p = 10 \log \frac{\sigma_{ori}}{\sigma_{pred}} \tag{14}$$

where, σ_{ori} and σ_{pred} are the variance of original signal and residual signal respectively. On the other hand, the entropy of the image can be determined by eqn (15):-

$$H = -\sum_{i=1}^{n} P_i \log_2 P_i \tag{15}$$

where P_i is the probability of occurrence of intensity value i. Since the entropy of image date dictates the theoretical lower bound of lossless compression rate achievable, we can assess the efficiency of different prediction model. The proposed method with the YLMN color transformation demonstrates the highest prediction gain and the lowest entropy, indicating a potential high compression efficiency. MEP2 can give

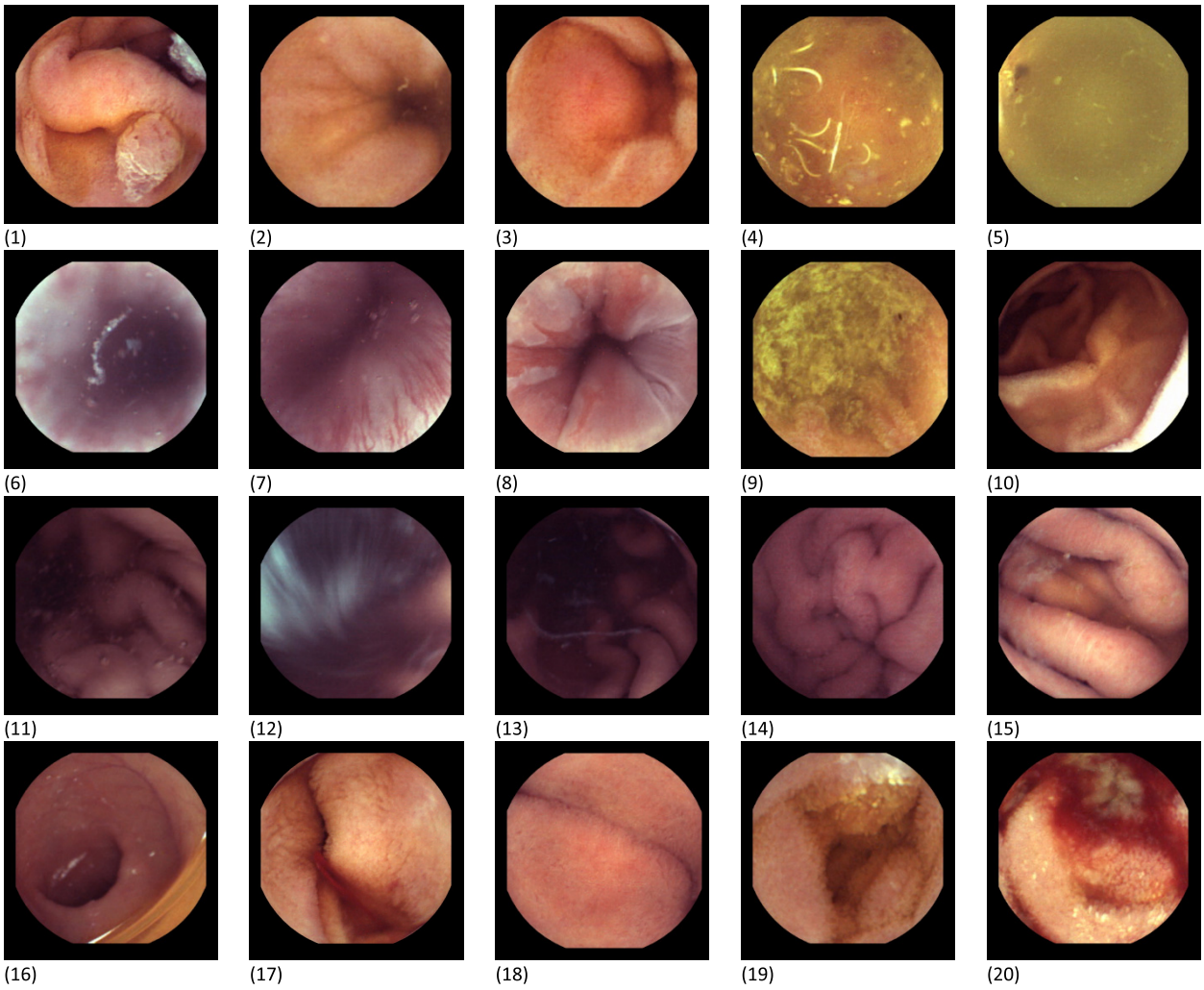

FIGURE 10. 20 (out of 100) test images taken from [25].

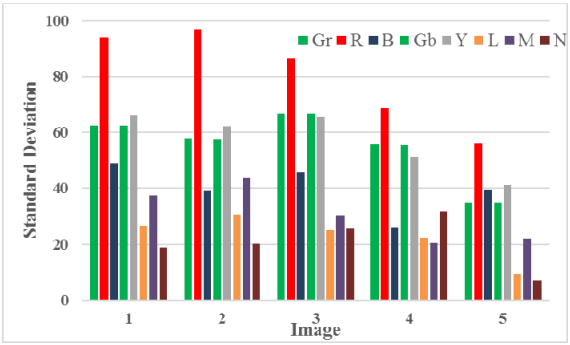

FIGURE 11. Comparison of standard deviation between the color components in original color space and YLMN color space.

a comparable result to our proposed method. However, as shown in Fig. 8, the prediction model in MEP2 requires storing two line of data for the prediction, while DPCM does not need any buffer memory. Therefore, the prediction model is expected to have lower memory requirement.

We have also analyzed the computational complexity in terms of normalized operations, such as addition (ADD), shift (SHF), comparison (CMP). We have also considered the buffer memory (MEM) requirements for the color space transformation and prediction computation. Table 2 shows the comparison. As expected, DPCM with horizontal prediction provides the lowest complexity and memory requirement. However, Fig. 12 shows the entropy is highest for DPCM model as the simple model can not exploit the inter-color correlation sufficiently. Both MEP1 and MEP2 offers better compression performance with an increase in computational complexity and buffer memory. However, by employing the YLMN color transformation, the proposed method smoothens the L, M and N channels. Thereby, it can give the best entropy and prediction gain. The increase in the computational complexity and buffer memory due to YLMN color transformation can be considered tolerable given that the proposed method yields reduction in average lossless bitrate of 0.2bpp as shown in Fig 12.

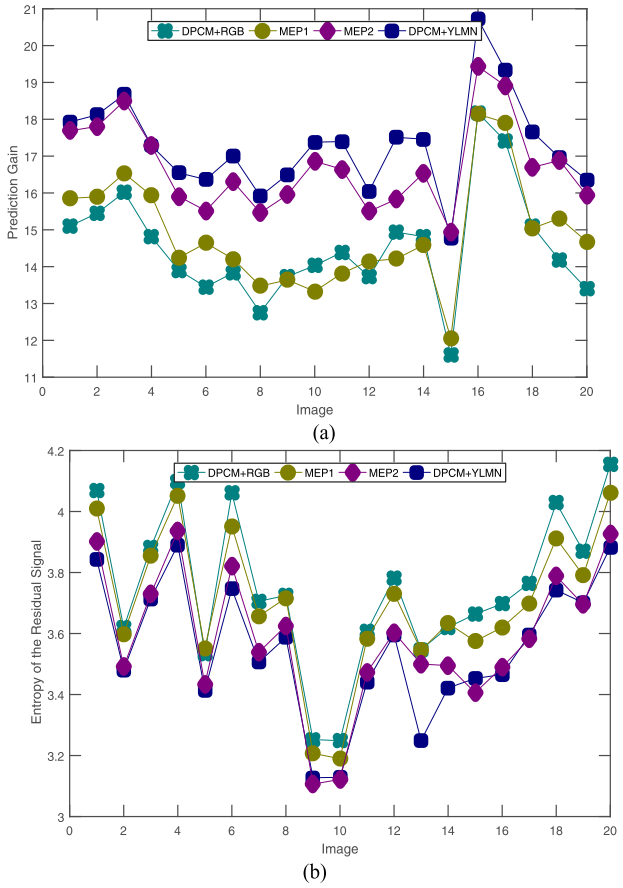

FIGURE 12. Comparison of (a) Prediction gain and (b) Entropy of sample images from the KID database with various prediction model.

TABLE 2. Number of operation per pixel required for various prediction model.

Prediction Model	ADD	SHF	CMP	Total	MEM
MEP1	2	0	7	9	2 x Width
MEP2	3	1	4	8	2 x Width
DPCM	1	0	0	1	0
Proposed Method	2.5	0	0	2.5	½ x Width

C. COMPRESSION PERFORMANCE

This section compares the coding performance of our proposed algorithm with standard lossless engine such as JPEG-2000 (J2K) and JPEG-LS (JLS), and also with recently proposed lossless compression algorithms for CE: cost-efficient lossless compression (CELC) [26], computationally efficient image compressor (CEIC) [11], and lossless image compression system (LICS) [10]. As JPEG-2000, JPEG-LS, LICS, and CEIC work on the full-color image, we have applied bilinear interpolation to interpolate the full-color image from the original CFA image. Then the full-color image was fed to these compression schemes, and the compression rate is measured by considering the size of original CFA image. Both CELC and our proposed method works directly on raw CFA image, therefore demosaicking is not used in these cases.

Except for J2K, all the other methods employ a predictive coding technique for lossless encoding. In LICS, an RGB demosaiced image is first mapped to YEF color space, which can capture the unique characteristics of endoscopic image compression. YEF color transformation reduces the complexity of color transformation as well as significantly improves the coding performance of the chrominance channel. Note should be taken that YEF color transformation is not integer reversible and requires up to 3 additional fraction bits for lossless color transformation. The lossless compression scheme in CEIC consists of a reversible color transformation YrUrVr, DPCM, and corner clipping. In CELC, the framework of JPEG-LS is modified for designing a cost-efficient image compressor for raw CFA image based on MEP2. The context template in the prediction model was modified to take account of the interleaved pixels in the raw CFA image. A hybrid encoder consists of Huffman and Golomb-Rice coder is used for efficient encoding of the residual error.

The output compression bitrates for CE images from KID Database achieved by various methods are listed in Table 3. Note should be taken that we have only implemented the prediction module MEP2 for CELC [26]. Due to unavailability of the complete Huffman tree for the encoder, we could not implement the encoder module. We have applied our encoder module on the residual signal to generate the result and compare with our method.

The results clearly illustrate that the algorithms based on a full-color image are not efficient for lossless encoding of raw CFA image. This indicates the compression stage cannot completely remove the redundancy added by the demosaicing stage. Among these methods, JPEG-LS gives the best result in terms of compression efficiency, outperforming second best LICS by 0.7 bpp.

On average, our proposed method with YLMN color transformation, Golomb-Rice coding and clipping can outperform all the other methods by achieving the lowest lossless compression of 3.53 bpp. Even without clipping, our proposed method has comparable results with CELC, which has a higher computational complexity as shown in Table 2.

Table 4 shows the comparison of the proposed method with other existing works on image compression for CE. For comparison, we have separated the algorithms in terms of 'demosaicking-first method' or 'compression-first method'. For the demosaicking-first method, we have listed here the reported results. Note should be taken that these reported results neglect the demosaicking error incurred, as well as hardware required to implement it on the image sensor end. However, for low compression ratios (compression ratio <10), demosaicking error dominates the reconstruction error [7]. For the sake of fair comparison, demosaicking-first methods should include the demosaicking error.

To distinguish between the color transformation for full-color image and CFA image, three components are used for full-color image and four components are used for CFA color transformation. For example, the original color space in the

TABLE 3. Lossless bitrate of various lossless compression scheme for CE (Two best results are marked in bold).

Image	J2K [36]	JLS [22]	LICS [10]	CEIC [11]	CELC [26]	Proposed		
						DPCM+GR	YLMN+ DPCM+GR	YLMN+DPCM+ GR+Clipping
1	7.01	5.71	7.07	9.98	4.15	4.31	**4.13**	**3.87**
2	6.50	5.21	6.73	9.44	**3.90**	4.08	3.95	**3.69**
3	6.18	4.95	6.54	9.03	**3.72**	3.98	3.83	**3.56**
4	6.93	5.67	7.14	9.72	4.13	4.27	**4.10**	**3.85**
5	6.06	4.82	6.22	8.64	**3.67**	3.81	3.68	**3.43**
6	6.71	5.42	6.96	9.64	4.07	4.28	**4.03**	**3.77**
7	6.31	5.03	6.64	9.19	3.88	4.06	**3.86**	**3.59**
8	6.67	5.36	6.76	9.49	3.96	4.08	**3.94**	**3.68**
9	5.62	4.52	6.17	8.16	**3.46**	3.68	3.53	**3.27**
10	4.91	3.94	5.67	7.18	**3.02**	3.33	3.15	**2.89**
11	5.33	4.30	5.92	7.84	**3.20**	3.47	3.32	**3.07**
12	5.06	4.08	5.65	7.29	**3.00**	3.21	3.12	**2.88**
13	6.00	4.82	6.19	8.68	**3.57**	3.79	3.68	**3.41**
14	6.56	5.28	6.67	9.45	3.94	4.11	**3.93**	**3.67**
15	4.78	3.87	5.61	6.85	**2.74**	2.89	2.88	**2.65**
16	5.63	4.49	6.07	8.21	**3.35**	3.70	3.43	**3.28**
17	6.33	5.08	6.62	9.26	3.84	4.09	**3.82**	**3.66**
18	6.68	5.40	6.96	9.68	4.10	4.35	**4.09**	**3.81**
19	6.72	5.43	7.12	9.97	4.06	4.36	**4.04**	**3.88**
20	7.07	5.71	7.27	10.11	4.20	4.41	**4.18**	**3.92**
Avg	6.25	5.05	6.58	8.99	3.75	3.95	**3.73**	**3.53**

TABLE 4. Comparison with other compression schemes.

Framework	Compression Type	Work	Colour Transformation	Algorithm	Compression Rate (bits per pixel)	PSNR (dB)
Demosaicking-First	Lossy	Li et. al. [31]	RGB	DCT	5.91	47.7
		Fante et. al. [11]	YUV	Prediction	2.32	40.6
	Lossless	Khan et al[24]	YUV	Prediction	6.48	∞
		Khan et al. (LICS) [10]	YEF	Prediction	5.28	∞
		Fante et al (CEIC) [11]	YUV	Prediction	6.33	∞
Compression-First	Lossy	Wahid et. al. [27]	GRBG	DCT	1.03	32.9
		Turzca et. al. [28]	YCoCgY	DCT	0.77	36.5
		Lin et. al. [29]	GRBG	DCT	1.63	32.5
		Dung et. al. [30]	GRBG	DCT	1.44	36.2
		Lin et. al. [32]	GRBG	DCT	1.42	40.7
		Chen et. al[12]	GRBG	Prediction	3.46	46.4
		Turzca et. al. [33]	YCuCvY	DCT	0.70	35.7
		Liu et. al. [14]	GRBG	Prediction	3.46	46.3
	Lossless	Chen et. al. (CELC) [26]	GRBG	Prediction	5.49	∞
		Proposed	YLMN	Prediction	**3.53**	∞

full-color image is denoted as RGB, while the companion color transformation in CFA is denoted as GRBG.

From the observed results, it is evident our proposed algorithm can give the lowest bitrate among all the other lossless compression algorithm. The lossless bitrate of proposed algorithm is greater than or comparable to the near-lossless (PSNR>46dB) bitrate achieved by compression-first algorithms such as [12] and [14]. Demosaicking-first

TABLE 5. Comparison with other compression-first lossless encoders for CE.

	Chen et. al. [12]	Chen et. al. [34]	Tsai et. al. [35]	CELC [26]	This Work
Process(um)	0.180	0.180	0.180	0.180	0.065
Frequency	20~24	20	200	200	250
Resolution	640	640	640	640	640
Gate Counts(k)	19.5	50	11.57	5.54	3.78
Memory(k)	17.5	29	15.2	10.2	2.93
Power(mW)	1.3	3.5	4.1	2.2	0.94
Normalized area	5.16	13.23	3.06	1.46	1

Note: The normalized core area is normalized by the NAND-equivalent gate counts.

methods such as [11] reported a better compression rate. However, this method neglects the demosaicking error, which has a significant effect in near-lossless compression [7].

Apart from the lossless bitrate, we also assess the computational complexity of the proposed compression method. To this end, this work is realized by using a hardware description language (HDL) Verilog and an EDA tool Design Compiler is used to synthesize the proposed design by TSMC 65 n*m* CMOS process. The gate counts of this work are only 3.78 k, and the core area is 29,627.28 (um $\times$ um). The power consumption of this work is 0.9 mW simulated by using SYNOPSYS Design Compiler when it operated at 250 MHz. The ASIC implementation of the design is built to check the utilization of resources and compare with the other compression-first algorithms. The resolution of the image used in this implementation is 640 $\times$ 640.

The reported implementation of demosaicking methods such as [10], [11], and [24] neglected the implementation cost of demosaicking process. However, high-quality hardware-oriented implementation of demosaicking process can take significant amount of gate counts, memory area and power [37]. Therefore for fair comparison, only compression-first methods are considered here.

Table 5 shows the comparison with other compression first encoder for CE. Our implementation reduces the gate counts by 38.9% and memory requirement by 71.2% than the previous design. The underlying reasons can be summarized as: (i) application of low complexity DPCM prediction model with a low complexity YLMN color transformation to exploit both spectral and spatial redundancy, (ii) usage of a memory efficient Golomb-Rice coder instead of a Huffman Coder, (iii) application of a low complexity corner clipping mechanism to cut the uninformative regions in the corner.

V. CONCLUSION

In this paper, we proposed a novel lossless image compression scheme for wireless capsule endoscopy system. The proposed system utilizes an optimum reversible color transformation to reduce the spectral redundancy in the image and adopts a low memory DPCM prediction model to reduce the spatial redundancy in the image. An adaptive Golomb-Rice encoder then compresses generated residual signal with single context with low computational complexity and memory requirement. A corner clipper scheme further reduces the lossless bitrate by removing the uninformative corner regions in the image. Experimental result shows that the proposed algorithm outperforms other lossless compression algorithms in terms of lossless compression rate, gate counts, and memory requirement.

REFERENCES

[1] G. Iddan, G. Meron, A. Glukhovsky, and P. Swain, "Wireless capsule endoscopy," *Nature*, vol. 405, no. 6785, pp. 417–418, May 2000.
[2] A.-M. Singeap, C. Stanciu, and A. Trifan, "Capsule endoscopy: The road ahead," *World J. Gastroenterol.*, vol. 22, no. 1, pp. 369–378, 2016.
[3] A. Karargyris and N. Bourbakis, "Wireless capsule endoscopy and endoscopic imaging: A survey on various methodologies presented," *IEEE Eng. Med. Biol. Mag.*, vol. 29, no. 1, pp. 72–83, Jan./Feb. 2010.
[4] A. Menciassi, G. Ciuti, and C. Cavallotti, "Future developments of video capsule endoscopy: Hardware," in *Video Capsule Endoscopy*. Berlin, Germany: Springer, 2014, pp. 543–556.
[5] D. K. Iakovidis and A. Koulaouzidis, "Software for enhanced video capsule endoscopy: Challenges for essential progress," *Nature Rev. Gastroenterol. Hepatol.*, vol. 12, no. 3, pp. 172–186, 2015.
[6] B. E. Bayer, "Color imaging array," U.S. Patent 3 971 065, Jul. 1976
[7] N.-X. Lian, L. Chang, V. Zagorodnov, and Y.-P. Tan, "Reversing demosaicking and compression in color filter array image processing: Performance analysis and modeling," *IEEE Trans. Image Process.*, vol. 15, no. 11, pp. 3261–3278, Nov. 2006.
[8] D. Hudesman, J. Mazurek, and A. Swaminath, "Capsule endoscopy in Crohn's disease: Are we seeing any better?" *World J. Gastroenterol.*, vol. 20, no. 36, pp. 13044–13051, 2014.
[9] C. Spada, M. E. Riccioni, R. Urgesi, and G. Costamagna, "Capsule endoscopy in celiac disease," *World J. Gastroenterol.*, vol. 14, no. 26, pp. 4146–4151, 2008.
[10] T. H. Khan and K. A. Wahid, "Design of a lossless image compression system for video capsule endoscopy and its performance in *in-vivo* trials," *Sensors*, vol. 14, no. 11, pp. 20779–20799, 2014.
[11] K. A. Fante, B. Bhaumik, and S. Chatterjee, "Design and implementation of computationally efficient image compressor for wireless capsule endoscopy," *Circuits, Syst. Signal Process.*, vol. 35, no. 5, pp. 1677–1703, 2016.
[12] X. Chen *et al.*, "A wireless capsule endoscope system with low-power controlling and processing ASIC," *IEEE Trans. Biomed. Circuits Syst.*, vol. 3, no. 1, pp. 11–22, Feb. 2009.
[13] X. Xie *et al.*, "A novel low power IC design for bi-directional digital wireless endoscopy capsule system," in *Proc. IEEE Int. Workshop Biomed. Circuits Syst.*, Dec. 2004, pp. S1-8–S1-8.
[14] G. Liu, G. Yan, S. Zhao, and S. Kuang, "A complexity-efficient and one-pass image compression algorithm for wireless capsule endoscopy," *Technol. Health Care*, vol. 23, no. s2, pp. S239–S247, 2015.
[15] H. S. Malvar and G. J. Sullivan, "Progressive-to-lossless compression of color-filter-array images using macropixel spectral-spatial transformation," in *Proc. Data Compress. Conf.*, Apr. 2012, pp. 3–12.
[16] H. S. Malvar, G. J. Sullivan, and S. Srinivasan, "Lifting-based reversible color transformations for image compression," *Proc. SPIE*, vol. 7073, p. 707307, Sep. 2008.
[17] N. Jayant and P. Noll, *Digital Coding of Waveforms Principles and Application to Speech and Video*. Englewood Cliffs, NJ, USA: Prentice-Hall, 1984.
[18] D. Lee and K. N. Plataniotis, "Lossless compression of HDR color filter array image for the digital camera pipeline," *Signal Process., Image Commun.*, vol. 27, no. 6, pp. 637–649, 2012.
[19] S. Kim and N. I. Cho, "Hierarchical prediction and context adaptive coding for lossless color image compression," *IEEE Trans. Image Process.*, vol. 23, no. 1, pp. 445–449, Jan. 2014.
[20] K. Chung and Y. Chan, "A lossless compression scheme for Bayer color filter array images," *IEEE Trans. Image Process.*, vol. 17, no. 2, pp. 134–144, Feb. 2008.
[21] Y. Gu, X. Xie, G. Li, T. Sun, and Z. Wang, "Two-stage wireless capsule image compression with low complexity and high quality," *Electron. Lett.*, vol. 48, no. 25, pp. 1588–1589, Dec. 2012.

[22] M. J. Weinberger, G. Seroussi, and G. Sapiro, "The LOCO-I lossless image compression algorithm: Principles and standardization into JPEG-LS," *IEEE Trans. Image Process.*, vol. 9, no. 8, pp. 1309–1326, Aug. 2000.
[23] S. W. Golomb, "Run-length encodings," *IEEE Trans. Inf. Theory*, vol. 53, no. 9, pp. 1689–1699, Sep. 1965.
[24] T. H. Khan and K. A. Wahid, "Lossless and low-power image compressor for wireless capsule endoscopy," *VLSI Des.*, vol. 2011, Jan. 2011, Art. no. 343787.
[25] D. K. Koulaouzidis and A. Iakovidis. (2016). *KID, A Capsule Endoscopy Database for Medical Decision Support*. [Online]. Available: http://is-innovation.eu/kid
[26] S.-L. Chen, Y.-R. Chen, T.-L. Lin, and Z.-Y. Liu, "A cost-efficient lossless compression color filter array images VLSI design for wireless capsule endoscopy," *J. Med. Imag. Health Inf.*, vol. 5, no. 2, pp. 378–384, 2015.
[27] K. Wahid, S.-B. Ko, and D. Teng, "Efficient hardware implementation of an image compressor for wireless capsule endoscopy applications," in *Proc. IEEE Int. Joint Conf. Neural Netw. (IJCNN)*, Jun. 2008, pp. 2761–2765.
[28] P. Turcza and M. Duplaga, "Low-power image compression for wireless capsule endoscopy," in *Proc. IEEE Int. Work. Imag. Syst. Techn. (IST)*, May 2007, pp. 1–4.
[29] M.-C. Lin, L.-R. Dung, and P.-K. Weng, "An ultra-low-power image compressor for capsule endoscope," *Biomed. Eng.*, vol. 5, no. 1, p. 14, 2006.
[30] L.-R. Dung, Y.-Y. Wu, H.-C. Lai, and P.-K. Weng, "A modified H.264 intra-frame video encoder for capsule endoscope," in *Proc. IEEE Biomed. Circuits Syst. Conf.*, Nov. 2008, pp. 61–64.
[31] J. Li and Y. Deng, "Fast compression algorithms for capsule endoscope images," in *Proc. 2nd Int. Congr. Image Signal Process.*, 2009, pp. 1–4.
[32] M.-C. Lin and L.-R. Dung, "A subsample-based low-power image compressor for capsule gastrointestinal endoscopy," *EURASIP J. Adv. Signal Process.*, vol. 2011, no. 1, p. 257095, 2011.
[33] P. Turcza and M. Duplaga, "Hardware-efficient low-power image processing system for wireless capsule endoscopy," *IEEE J. Biomed. Health Inform.*, vol. 17, no. 6, pp. 1046–1056, Nov. 2013.
[34] X. Chen, H. Jiang, X. Li, and Z. Wang, "A novel compression method for wireless image sensor node," in *Proc. IEEE Asian Solid-State Circuits Conf.*, Nov. 2007, pp. 184–187.
[35] T. H. Tsai, Y. H. Lee, and Y. Y. Lee, "Design and analysis of high-throughput lossless image compression engine using VLSI-oriented FELICS algorithm," *IEEE Trans. Very Large Scale Integr. (VLSI) Syst.*, vol. 18, no. 1, pp. 39–52, Jan. 2010.
[36] C. Christopoulos, A. Skodras, and T. Ebrahimi, "The JPEG2000 still image coding system: An overview," *IEEE Trans. Consum. Electron.*, vol. 46, no. 4, pp. 1103–1127, Nov. 2000.
[37] S.-L. Chen and H.-R. Chang, "Fully pipelined low-cost and high-quality color demosaicking VLSI design for real-time video applications," *IEEE Trans. Circuits Syst. II, Exp. Briefs*, vol. 62, no. 6, pp. 588–592, Jun. 2015.
[38] M. D. Adams, F. Kossentini, and R. K. Ward, "Generalized S transform," *IEEE Trans. Signal Process.*, vol. 50, no. 11, pp. 2831–2842, Nov. 2002.

SHAHED K. MOHAMMED (S'15) received the B.S. degree (Hons.) in electrical and electronic engineering from the Bangladesh University of Engineering and Technology, Dhaka, Bangladesh, in 2013, and the M.Sc. degree from the University of Saskatchewan, Saskatoon, Canada, in 2017. From 2013 to 2014, he served as a Lecturer with United International University, Dhaka. His research interest includes medical imaging, computer-aided detection system, wireless implantable, and wireless capsule endoscopy system.

Mr. Mohammed received the CGSR Scholarship (University of Saskatchewan) and the Dean Scholarship (Bangladesh University of Engineering and Technology).

K. M. MAFIJUR RAHMAN was born in 1991. He received the B.Sc. degree from the Department of Electrical and Electronic Engineering, Bangladesh University of Engineering and Technology, Dhaka, Bangladesh, in 2014. He was a Secretary with the IEEE BUET Student Branch from 2012 to 2013. He is currently pursuing the M.Sc. degree with the Department of Electrical Engineering, University of Saskatchewan, Canada. His research interest includes Bayer color filter image, color transform, compression algorithm, and hardware implementation.

KHAN A. WAHID (S'02–M'07–SM'13) received the B.Sc. degree from the Bangladesh University of Engineering and Technology in 2000, and the M.Sc. and Ph.D. degrees from the University of Calgary in 2003 and 2007, respectively. He is currently a Professor with the Department of Electrical and Computer Engineering, University of Saskatchewan. He has co-authored two book chapters and over 140 peer-reviewed journal and international conference papers in the field of video and image processing, embedded systems, Internet of Things, medical imaging, and health informatics. He has two patents. He is a registered Professional Engineer at Saskatchewan. He received many prestigious awards and scholarships, including the Most Distinguished Killam Scholarship and the NSERC Canada Graduate Scholarship for his doctoral research, and the Award of Innovation from Innovation Place in 2016.